Science and Technology Indonesia
e-ISSN:2580-4391 *p*-ISSN:2580-4405
Vol. 10, No. 1, January 2025

Research Paper

Electrospun Rare-Earth Metal Oxide (CeO_2) Nanofiber for the Degradation of Congo Red Aqueous Dyes

Aditya Rianjanu[1,2*], Trivendi Haloho[1], Joshua Leonardo Pasaribu[1], Achmad Gus Fahmi[2,3], Eka Nurfani[1], Wahyu Solafide Sipahutar[1], Hadi Teguh Yudistira[2,4], Tarmizi Taher[2,5*]

[1]*Department of Materials Engineering, Faculty of Industrial Technology, Institut Teknologi Sumatera, Lampung Selatan, 35365, Indonesia*
[2]*Center for Green and Sustainable Materials, Institut Teknologi Sumatera, Lampung Selatan 35365, Indonesia*
[3]*Department of Cosmetic Engineering, Faculty of Industrial Technology, Institut Teknologi Sumatera, Lampung Selatan, 35365, Indonesia*
[4]*Department of Mechanical Engineering, Faculty of Industrial Technology, Institut Teknologi Sumatera, Lampung Selatan, 35365, Indonesia*
[5]*Department of Environmental Engineering, Faculty of Infrastructure and Regional Technology, Institut Teknologi Sumatera, Lampung Selatan, 35365, Indonesia*
*__Corresponding author__: aditya.rianjanu@mt.itera.ac.id (AR), tarmizi.taher@tl.itera.ac.id (TT)

Abstract
The persistent presence of organic dyes like Congo Red (CR) in wastewater poses a significant environmental challenge. In this study, CeO_2 nanofibers (CeO_2-NF) were successfully synthesized via electrospinning followed by calcination as potential photocatalysts for the degradation of CR pollutants in aqueous solutions. The synthesized nanofibers were characterized using field emission scanning electron microscopy coupled with energy dispersive X-Ray Spectroscopy (FESEM-EDS) for morphological and elemental analyses, X-Ray Diffraction (XRD) for crystalline structure, and Fourier transform infrared (FTIR) spectroscopy for molecular properties. Photocatalytic degradation experiments were conducted under UVC light irradiation, with the CeO_2-NF1, CeO_2-NF2, and CeO_2-NF3 samples achieving CR degradation percentages of 95.6%, 96.9%, and 95.2%, respectively, after 130 minutes of reaction time. Kinetic analysis revealed that the photocatalytic degradation followed pseudo-first-order kinetics, with rate constants of 0.020 min^{-1}, 0.024 min^{-1}, and 0.025 min^{-1} for CeO_2-NF1, CeO_2-NF2, and CeO_2-NF3, respectively, highlighting the superior performance of CeO_2-NF3. These results indicate that CeO_2NF could serve as an effective material for the photocatalytic degradation of organic dyes, offering a promising approach for wastewater treatment applications.

Keywords
Wastewater Treatment, Cerium Oxide, Electrospinning, Calcination, Photocatalyst

Received: 1 July 2024, Accepted: 14 October 2024
https://doi.org/10.26554/sti.2025.10.1.123-130

1. INTRODUCTION

The presence of synthetic dyes in industrial wastewater has become an environmental concern due to their toxicity, stability, and poor biodegradability (Srivastava et al., 2022; Thakare et al., 2022). Synthetic dyes are extensively used in various industries, including textiles, leather, plastics, cosmetics, and pharmaceuticals, leading to large volumes of dye-contaminated wastewater being released into the environment (Fried et al., 2022). Once released into water bodies, these dyes pose serious environmental and health risks because they resist natural degradation processes and can persist for long periods (Tkaczyk et al., 2020). Among these dyes, Congo Red (CR) is a carcinogenic anionic dye commonly used in the textile, paper, and plastic industries, and it poses a significant challenge in water treatment (Hasanah et al., 2022; Mohadi et al., 2017; Oladoye et al., 2022). Traditional methods for removing such dyes, such as adsorption, coagulation, and biological degradation, often fall short in efficiency, cost, or environmental impact (Ahmad et al., 2024; Chouchane et al., 2024; Dutta et al., 2021; Sriram et al., 2022). As a result, there is a growing interest in developing novel materials capable of efficiently removing or degrading these pollutants.

Photocatalytic degradation has emerged as an attractive approach to address this problem due to its potential for complete mineralization of organic pollutants into non-toxic byproducts (Tang et al., 2022; Zhang et al., 2020; Zhao et al., 2022). Various materials have been explored as so-called first generation photocatalysts (i.e., ZnO, TiO_2, SnO_2, MnO_2, Fe_2O_3, NiO, and WO_3 and CeO_2) (Krishnan et al., 2024; Rianjanu et al., 2024b,a,c). Among them, cerium oxide (CeO_2) offers unique advantages, such as high oxidative ability, chemical stability, and non-toxicity (Anandkumar et al., 2017; Fauzi et al., 2022; Kumar et al., 2024; Matussin et al., 2023; Mylarappa

et al., 2024; Rianjanu et al., 2024d). Various methods have been developed to fabricate CeO_2 nanostructured materials as photocatalytic materials. Common techniques include sol-gel synthesis, hydrothermal or solvothermal methods, precipitation, and electrospinning, each offering different advantages in terms of particle size control, crystallinity, and surface area (Cam et al., 2022; Montini et al., 2016). Among these methods, electrospinning has emerged as a versatile and simple technique for fabricating CeO_2 nanofibers with unique properties (Yang et al., 2022).

Electrospinning involves the application of a high voltage to a polymer solution containing metal precursors, which results in the formation of fine fibers (Almafie et al., 2024; Kusumawati et al., 2024). These fibers are then subjected to a calcination process to remove the polymer matrix, leaving behind highly porous and crystalline CeO_2 nanofibers (Mondal and Sharma, 2016). This method is particularly attractive for photocatalytic applications due to the large surface area-to-volume ratio, enhanced porosity, and interconnected network of the resulting nanofibers, all of which improve the interaction between the photocatalyst and pollutants (Yaipimai et al., 2015; Yanalak et al., 2018). The combination of simplicity, scalability, and the ability to tune fiber properties makes electrospinning a promising approach for the fabrication of CeO_2-based photocatalytic materials.

In this study, we aim to synthesize CeO_2 nanofibers (CeO_2-NF) via electrospinning followed by calcination and evaluate their photocatalytic performance for the degradation of Congo Red dye under UVC light irradiation. Electrospinning offers a simple method to fabricated metal oxide nanofiber followed by calcinations process (Mondal and Sharma, 2016; Yang et al., 2022). The synthesized nanofibers will be characterized using Field-Emission Scanning Electron Microscopy coupled with Energy Dispersive X-Ray (FESEM-EDS), X-Ray Diffraction (XRD), and Fourier Transform Infrared Spectroscopy (FTIR) to assess their morphological, elemental, crystalline, and molecular properties, respectively. The efficacy of these nanofibers for dye degradation could offer a sustainable and efficient alternative for wastewater treatment.

2. EXPERIMENTAL SECTION

2.1 Materials

Cerium nitrate hexahydrate ($Ce(NO_3)_3{\cdot}6H_2O$, Merck) was used as the cerium precursor for the synthesis of cerium oxide (CeO_2) nanofibers. Polyvinylpyrrolidone (PVP, Sigma-Aldrich) served as the polymer matrix, assisting in the formation of nanofibers during electrospinning. N,N-Dimethylformamide (DMF, Merck) and ethanol (Merck) were employed as solvents to dissolve the cerium nitrate and PVP, ensuring a homogeneous precursor solution for electrospinning. Congo red (CR, Merck) was used as the target pollutant for evaluating the photocatalytic activity of the synthesized CeO_2 nanofibers. All chemicals were used without further purification.

2.2 Methods

CeO_2 nanofibers hereafter refer as CeO_2-NF were synthesized via an electrospinning process, as illustrated in Figure 1. Initially, 0.324 g of cerium nitrate hexahydrate was dissolved in 5 mL of a 50:50 (v/v) mixture of N,N-dimethylformamide (DMF) and ethanol. The solution was stirred at 60 °C and 600 rpm for 1 hour to ensure complete dissolution of the cerium nitrate. Subsequently, 0.535 g of polyvinylpyrrolidone (PVP) was added to the solution, which was stirred for an additional 2 hours until a transparent, homogeneous, and viscous solution was obtained. This precursor solution was then subjected to electrospinning under predetermined parameters: a voltage of 10 kV, a tip-to-collector distance of 15 cm, and a spinning duration of 6 hours. The resulting PVP/$Ce(NO_3)_3$ membrane was calcined at 500 °C for 2 hours, leading to the formation of CeO_2 nanofibers, referred to as CeO_2-NF1. For the synthesis of the other variants, CeO_2-NF2 and CeO_2-NF3, the same procedure was followed, with the exception of the cerium nitrate hexahydrate content, which was adjusted to 0.434 g and 0.540 g, respectively.

For the photocatalytic experiments, 25 mg of each CeO_2-NF sample was utilized. A 10 mg/L solution of Congo red (CR) was prepared by dissolving the dye in 100 mL of distilled water. The photodegradation experiments were conducted in a chamber equipped with a magnetic stirrer and illuminated by two 10 W UVC lamps (Phillips TUV), with a maximum emission wavelength of 274 nm. The CeO_2-NF samples were dispersed in the CR solution, and the mixture was stirred in the dark for 30 minutes to establish adsorption-desorption equilibrium. At the start of the reaction, a 3.5 mL aliquot was collected and subjected to UV-Vis spectrophotometric analysis (Shimadzu UV-1200) to determine the initial CR concentration. Subsequent 3.5 mL aliquots were withdrawn at specific time intervals throughout the 130-minute reaction period for UV-Vis measurements to monitor the dye degradation.

3. RESULT AND DISCUSSION

3.1 CeO_2-NF Characterizations

Figure 2 presents the FESEM images and corresponding EDS analyses of the CeO_2-NF samples synthesized via electrospinning, followed by calcination. Figure 2(a,e) displays the FE-SEM image of the uncalcined PVP/$Ce(NO_3)_3$ nanofibers (CeO_2-NF precursor), which exhibit a smooth and continuous morphology with an average fiber diameter of approximately 210 nm, consistent with previous reports (Sukowati et al., 2023). This confirms the success of the electrospinning process. After the calcination process, the nanofiber membranes transform into a powder-like structure, as a result of the complete decomposition of the PVP matrix, which aligns with previous studies (Huang et al., 2018; Jian et al., 2022; Yang et al., 2019). The post-calcination morphology of the CeO_2-NF is shown in Figure 2(b-h). In contrast to the smooth surface observed in the uncalcined nanofibers (Figure 2(a,e)), the calcined fibers exhibit a rougher surface texture, marked by significant porosity especially observed in Figure 2(f) to 2(h). The presence of

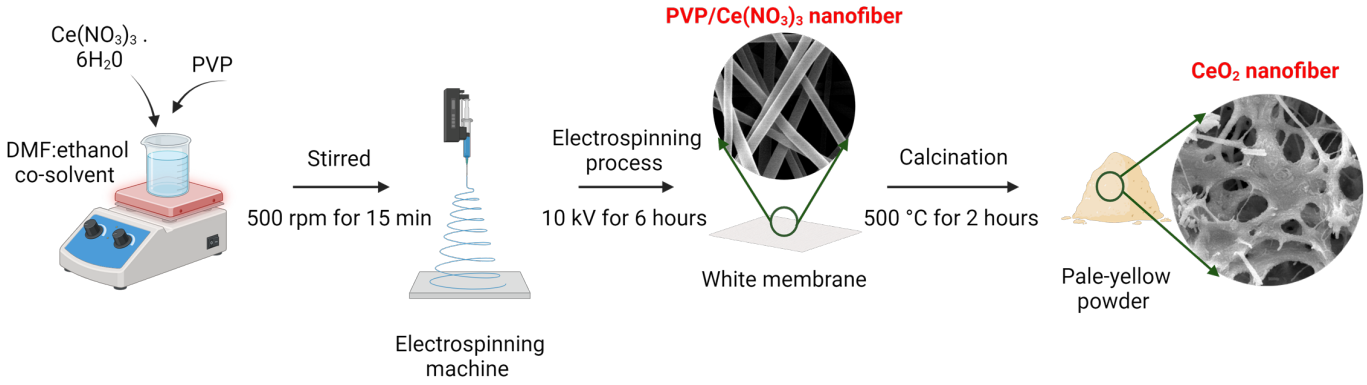

Figure 1. Schematic Illustration of the Cerium Dioxide Nanofiber (CeO_2-NF) Fabrication Process Using Electrospinning Method Followed by Calcination

large voids and junctions is attributed to the thermal decomposition of organic components during calcination. The selected calcination temperature of 500 °C effectively removed these organic elements, while preserving the overall integrity of the nanofiber framework.

The EDS elemental mapping results, shown in Figure 2(i), reveal the distribution of carbon (C), nitrogen (N), oxygen (O), and cerium (Ce) across the CeO_2-NF1, CeO_2-NF2, and CeO_2-NF3 samples. Minimal carbon and nitrogen are detected in all three samples, indicating that the calcination process successfully removed most of the organic PVP matrix from PVP/$Ce(NO_3)_3$ structure. The low levels of residual carbon and nitrogen suggest effective polymer decomposition, with only trace amounts remaining, possibly due to incomplete combustion or surface contamination. Oxygen is uniformly distributed and present in significant amounts, as expected in the CeO_2-NF structure. The strong and consistent oxygen signal across all samples supports the successful formation of cerium oxide. Similarly, cerium is well-dispersed in all the nanofibers, which is essential for ensuring consistent photocatalytic activity.

The quantitative atomic composition, depicted in Figure 2(j), further supports these observations. Carbon and nitrogen contents are considerably lower than those of oxygen and cerium, confirming the near-complete removal of organic components following calcination. Oxygen and cerium dominate the elemental composition, with a higher oxygen-to-cerium ratio in CeO_2-NF1 and CeO_2-NF3, suggesting the presence of oxygen vacancies. These vacancies are known to enhance photocatalytic performance by improving charge separation and promoting the generation of reactive oxygen species (ROS). In contrast, CeO_2-NF2 shows a slightly higher cerium content relative to oxygen, implying a more cerium-rich structure, which could lead to fewer oxygen vacancies and potentially different photocatalytic behavior compared to the other two samples. Overall, the uniform distribution of cerium and oxygen in the elemental maps, combined with the quantitative analysis, confirms the successful fabrication of CeO_2 nanofibers and highlights the potential role of oxygen vacancies in influencing photocatalytic efficiency.

Figure 3a presents the X-Ray Diffraction (XRD) spectra for all the CeO_2-NF samples. Distinct peaks are observed at 2θ values of 28°, 33°, 47°, 56°, 69°, 76°, 79°, and 88°, corresponding to the characteristic peaks of the face-centered cubic (FCC) structure of CeO_2, in accordance with JCPDS PDF#43-1002 (Liu et al., 2022). These peaks confirm the successful formation of crystalline cerium oxide nanofibers. However, additional peaks at 26°, 43°, and 51° are also present, corresponding to residual cerium oxide carbonate hydrate ($Ce_2(CO_3)_2O{\cdot}H_2O$), indicating that the carbonate species were not fully degraded during calcination in the CeO_2-NF sample. The crystallinity percentages for CeO_2-NF1, CeO_2-NF2, and CeO_2-NF3 were calculated to be 69.7%, 69.0%, and 75.0%, respectively, as shown in Figure 3b. The higher crystallinity of CeO_2-NF3 could be attributed to the higher precursor concentration used during synthesis, allowing for more pronounced crystal growth. While the higher crystallinity generally improves electron mobility and enhances photocatalytic performance, the presence of the secondary $Ce_2(CO_3)_2O{\cdot}H_2O$ phase in CeO_2-NF3 could potentially influence its catalytic efficiency by interfering with the pure CeO_2 phase. Overall, the XRD analysis confirms the successful preparation of highly crystalline CeO_2-NF via electrospinning followed by calcination.

The FTIR spectra in Figure 3(c) provide valuable insights into the chemical structure and bond formation in the CeO_2-NF samples compared to the PVP/$Ce(NO_3)_3$ precursor. In the precursor spectrum, characteristic peaks associated with PVP, and cerium nitrate are observed. The C=O stretching vibration from the PVP carbonyl group appears at 1662 cm^{-1}, while the C-N stretching vibration is seen near 1280 cm^{-1}. A strong peak at 1380 cm^{-1} confirms the presence of nitrate ions (NO_3^-) from cerium nitrate (Pandey et al., 2020). After calcination, these organic-related peaks disappear from the CeO_2-NF spectra, indicating the complete decomposition of the PVP matrix during the heat treatment. The formation of cerium oxide

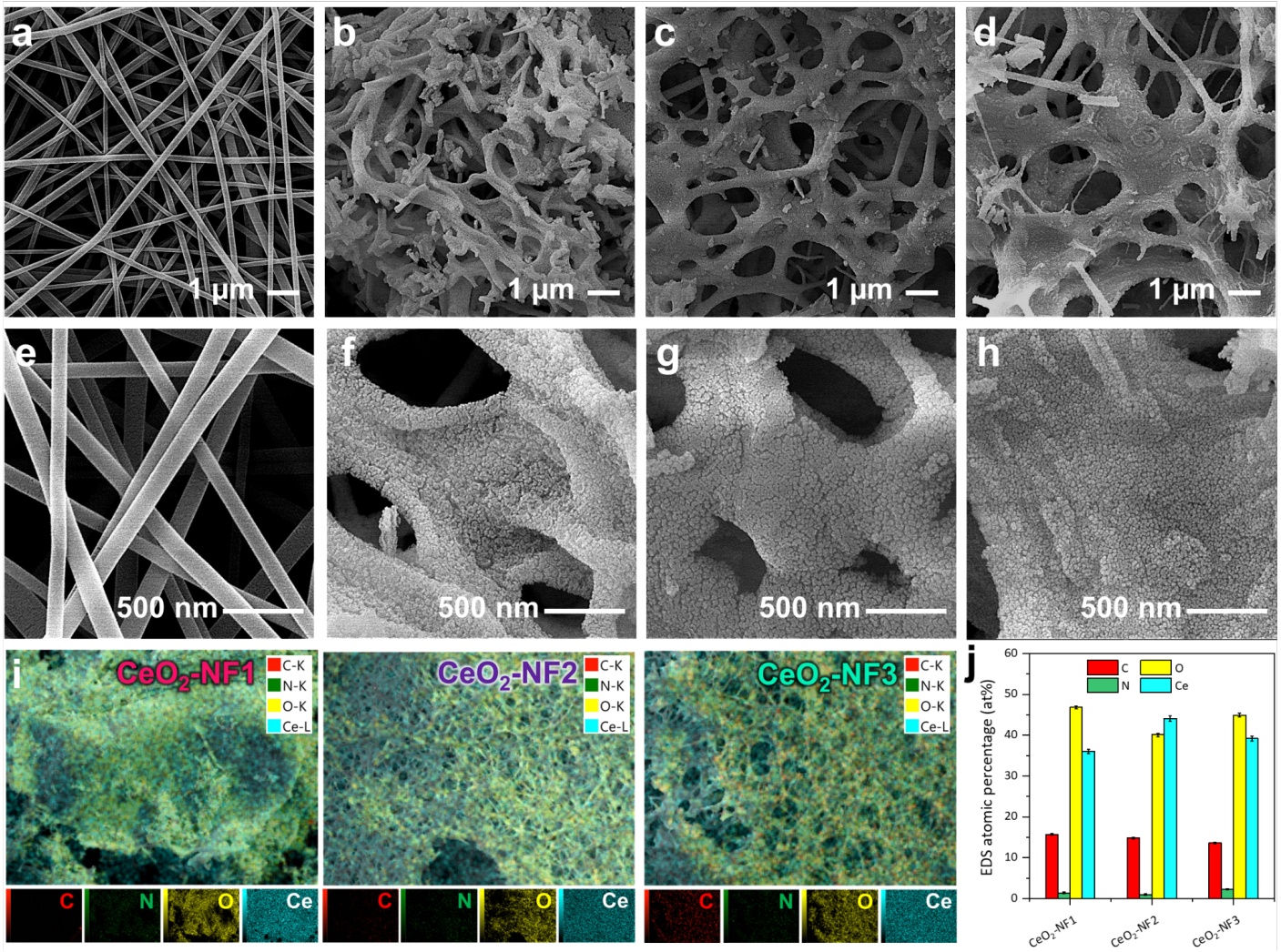

Figure 2. Field Emission Scanning Electron Microscopy (FESEM) Images of the anofibers: (a, e) PVP/$Ce(NO_3)_3$ precursor fibers, (b, f) CeO_2-NF1, (c, g) CeO_2-NF2, and (d, h) CeO_2-NF3 After Calcination. (i) EDS Elemental Mapping of the CeO_2-NF1, CeO_2-NF2, and CeO_2-NF3 Sample, Indicating the Distribution of Elements. (j) Quantitative EDS Analysis, Showing the Elemental Composition of the CeO_2-NF Samples

is confirmed by the appearance of new broad peaks between 400–600 cm^{-1}, corresponding to Ce−O stretching vibrations. These strong peaks verify the successful synthesis of CeO_2 nanofibers across all samples (Liu et al., 2015; Yan and Zhu, 2008).

The spectra for CeO_2-NF1, CeO_2-NF2, and CeO_2-NF3 are similar, indicating consistent CeO_2 formation across the different samples despite variations in precursor concentrations. This suggests that the structural transformation during calcination was uniform. Minor differences in peak intensity could be linked to slight variations in crystallinity or the presence of residual carbonates, though these do not significantly impact the FTIR spectra. Overall, the FTIR results confirm the successful decomposition of organic components and the formation of CeO_2-NF, aligning well with the XRD data.

3.2 Congo Red Photocatalytic Performance

The photocatalytic degradation capabilities of the CeO_2-NF samples were tested using Congo red (CR) as the model dye, and the results are presented in Figure 3(d-f). The CR aqueous solution exhibited a decrease in absorbance value as the reaction time with the CeO_2-NF catalyst increased. This indicates that the concentration of CR diminished over time under the influence of all CeO_2-NF samples, confirming their ability to accelerate the photocatalytic degradation of the CR dye. The degradation rate is illustrated in Figure 2g, where C represents the concentration of CR at any given time, and C_0 is the initial concentration of the CR dye (10 mg/L). The results show that after 50 minutes of contact, the remaining concentrations of the CR solution were 17%, 29%, and 36% for CeO_2-NF1, CeO_2-NF2, and CeO_2-NF3, respectively. When the reaction

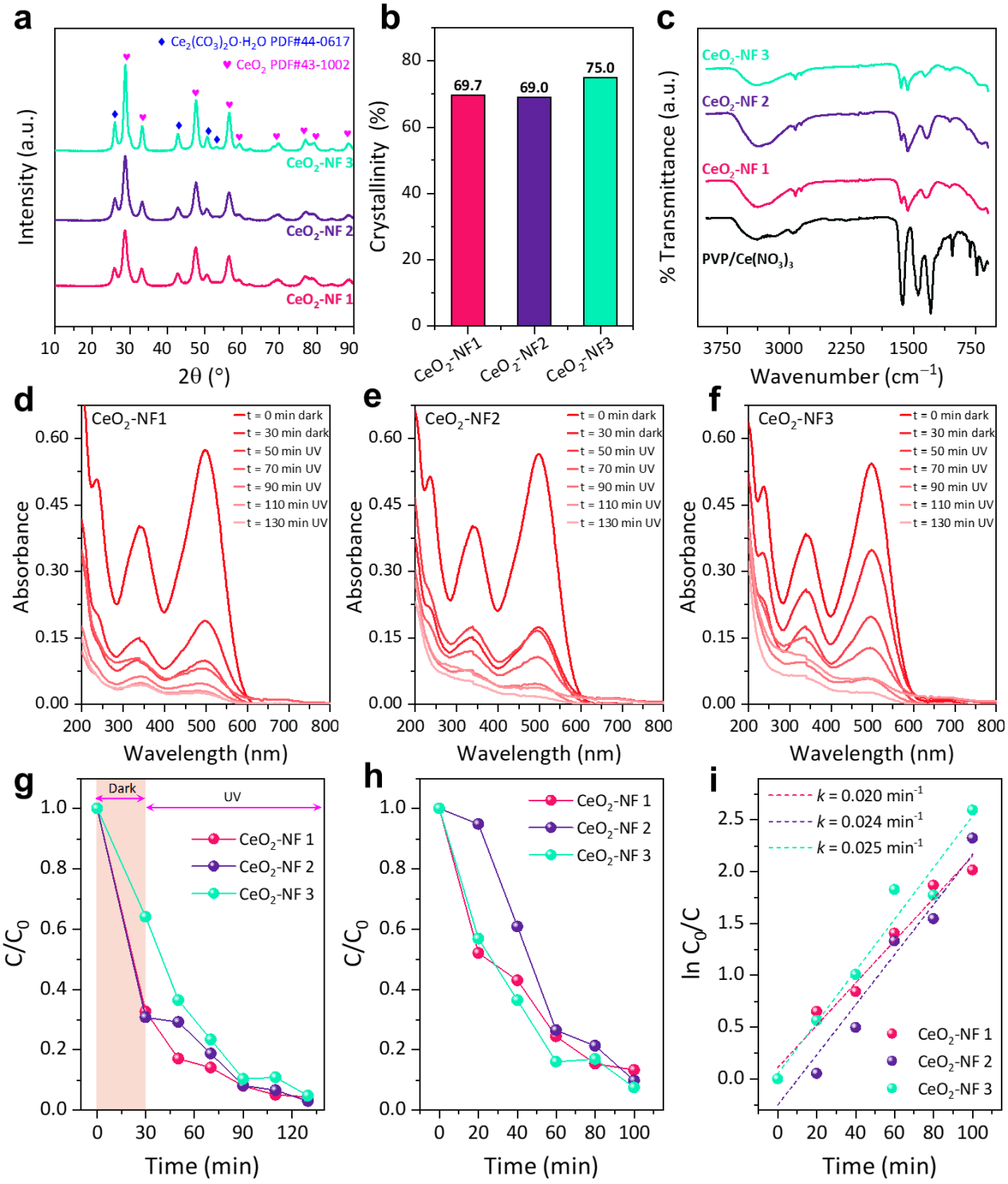

Figure 3. (a) X-Ray Diffraction (XRD) Patterns of CeO_2-NF Samples. (b) Crystallinity Percentages of the CeO_2-NF Samples. (c) FTIR Spectra Showing the Transmittance Profiles of CeO_2-NF, with the Characteristic Peaks of the PVP/$Ce(NO_3)_3$ Precursor Also Displayed for Comparison. UV-Vis Absorbance Spectra Showing the Degradation of Congo Red (CR) Dye Over Time Under UV Irradiation for (d) CeO_2-NF1, (e) CeO_2-NF2, and (f) CeO_2-NF3. Time-Dependent Photocatalytic Degradation of CR Dye Under (g) Full Condition (Dark + UV) and (h) UV Irradiation. (i) Kinetic Analysis of the CR Degradation Using a Pseudo-First-Order Reaction Model for CeO_2-NF

time was extended to 130 minutes, all three CeO_2-NF samples completely degraded the CR solution. The degradation percentages after 130 minutes were 95.6%, 96.9%, and 95.2% for CeO_2-NF1, CeO_2-NF2, and CeO_2-NF3, respectively. These findings demonstrate that the prepared CeO_2-NF samples are effective in degrading CR aqueous solutions, indicating their potential applicability in wastewater treatment technologies.

The results presented in Figure 3h show the time-dependent photocatalytic degradation of Congo Red (CR) dye under UV irradiation for the CeO_2-NF samples. During the initial 30-minute dark adsorption period, a slight reduction in CR concentration occurs due to adsorption on the nanofibers. Once UV light is applied, the dye concentration decreases rapidly, with CeO_2-NF3 exhibiting the highest degradation efficiency, followed by CeO_2-NF2 and CeO_2-NF1. The superior performance of CeO_2-NF3 can be attributed to its higher crystallinity and the potential presence of oxygen vacancies, which improve electron-hole separation and enhance photocatalytic activity. By the end of the 130-minute irradiation, CeO_2-NF3 achieves nearly complete degradation of the dye, highlighting its effectiveness.

In Figure 3i, the kinetic analysis of the photocatalytic degradation is modeled as a pseudo-first-order reaction. The rate constants (k) for CeO_2-NF1, CeO_2-NF2, and CeO_2-NF3 are 0.020 min^{-1}, 0.024 min^{-1}, and 0.025 min^{-1}, respectively, confirming that CeO_2-NF3 has the highest degradation rate, consistent with the results in Figure 3h. The linearity of the kinetic plot further confirms that the degradation follows pseudo-first-order kinetics, a common characteristic in photocatalytic processes. The differences in rate constants are linked to the structural properties of the nanofibers, with CeO_2-NF3 higher crystallinity and fewer impurities contributing to its superior photocatalytic performance.

4. CONCLUSIONS

CeO_2 nanofibers (CeO_2-NF) have been successfully fabricated through electrospinning, followed by a calcination process, to serve as photocatalytic materials for degrading aqueous Congo red (CR) pollutants. The synthesized CeO_2-NF samples were characterized using FESEM-EDS, XRD, and FTIR analyses to investigate their morphological, elemental, crystalline, and molecular properties, respectively. When tested as photocatalysts under UVC light, the CeO_2-NF samples exhibited high degradation efficiencies, with CR removal percentages of 95.6%, 96.9%, and 95.2% for CeO_2-NF1, CeO_2-NF2, and CeO_2-NF3, respectively, after 130 minutes of reaction time. The photocatalytic degradation followed pseudo-first-order kinetics, with the rate constants (k) determined to be 0.020 min^{-1}, 0.024 min^{-1}, and 0.025 min^{-1} for CeO_2-NF1, CeO_2-NF2, and CeO_2-NF3, respectively. These results demonstrate the effectiveness of the synthesized CeO_2-NF as photocatalytic materials, with high crystallinity, uniformity, and favorable kinetic performance contributing to their degradation efficiency. This study presents a promising approach for the development of advanced photocatalysts, potentially contributing to the advancement of wastewater treatment technologies.

5. ACKNOWLEDGMENT

The authors would like to acknowledge the invaluable contributions of Mr. Dedi Triyadi for his support and assistance throughout the research process. We would also like to thank the Institut Teknologi Sumatera, for providing the necessary resources and equipment for this study.

REFERENCES

Ahmad, N., A. Wijaya, F. S. Arsyad, I. Royani, and A. Lesbani (2024). Layered Double Hydroxide-Functionalized Humic Acid and Magnetite by Hydrothermal Synthesis for Optimized Adsorption of Malachite Green. *Kuwait Journal of Science*, **51**(2); 100206

Almafie, M. R., R. Dani, R. Riyanto, L. Marlina, J. Jauhari, and I. Sriyanti (2024). Preparation of PAN/PVDF Nanofiber Mats Loaded with Coconut Shell Activated Carbon and Silicon Dioxide for Lithium-Ion Battery Anodes. *Science and Technology Indonesia*, **9**(2); 427–447

Anandkumar, M., G. Vinothkumar, and K. Suresh Babu (2017). Synergistic Effect of Gold Supported on Redox Active Cerium Oxide Nanoparticles for the Catalytic Hydrogenation of 4-Nitrophenol. *New Journal of Chemistry*, **41**(14); 6720–6729

Cam, T. S., S. O. Omarov, M. I. Chebanenko, S. G. Izotova, and V. I. Popkov (2022). Recent Progress in the Synthesis of CeO_2-Based Nanocatalysts Towards Efficient Oxidation of CO. *Journal of Science: Advanced Materials and Devices*, **7**(1); 100399

Chouchane, T., M. T. Abedghars, S. Chouchane, and A. Boukari (2024). Improvement of the Sorption Capacity of Methylene Blue Dye Using Slag, a Steel By Product. *Kuwait Journal of Science*, **51**(2); 100210

Dutta, S., B. Gupta, S. K. Srivastava, and A. K. Gupta (2021). Recent Advances on the Removal of Dyes from Wastewater Using Various Adsorbents: A Critical Review. *Materials Advances*, **2**(14); 4497–4531

Fauzi, A. A., A. A. Jalil, N. S. Hassan, F. F. A. Aziz, M. S. Azami, I. Hussain, and D.-V. N. Vo (2022). A Critical Review on Relationship of CeO_2-Based Photocatalyst Towards Mechanistic Degradation of Organic Pollutant. *Chemosphere*, **286**; 131651

Fried, R., I. Oprea, K. Fleck, and F. Rudroff (2022). Biogenic Colourants in the Textile Industry – A Promising and Sustainable Alternative to Synthetic Dyes. *Green Chemistry*, **24**(1); 13–35

Hasanah, M., A. Wijaya, F. S. Arsyad, R. Mohadi, and A. Lesbani (2022). Preparation of Hydrochar from Salacca Zalacca Peels by Hydrothermal Carbonization: Study of Adsorption on Congo Red Dyes and Regeneration Ability. *Science and Technology Indonesia*, **7**(3); 372–378

Huang, J., X. Liu, G. Chen, N. Zhang, R. Ma, and G. Qiu

(2018). Selective Fabrication of Porous Iron Oxides Hollow Spheres and Nanofibers by Electrospinning for Photocatalytic Water Purification. *Solid State Sciences*, **82**; 24–28

Jian, S., Z. Tian, J. Hu, K. Zhang, L. Zhang, G. Duan, and S. Jiang (2022). Enhanced Visible Light Photocatalytic Efficiency of La-Doped ZnO Nanofibers via Electrospinning-Calcination Technology. *Advanced Powder Materials*, **1**(2); 100004

Krishnan, A., A. Swarnalal, D. Das, M. Krishnan, V. S. Saji, and S. M. A. Shibli (2024). A Review on Transition Metal Oxides Based Photocatalysts for Degradation of Synthetic Organic Pollutants. *Journal of Environmental Sciences*, **139**; 389–417

Kumar, H., A. Giri, and A. Rai (2024). Photocatalytic Degradation of Naphthol Blue Black Dye Using Undoped and Al-Doped Cobalt Ferrite Nanoparticles. *Kuwait Journal of Science*, **51**(2); 100208

Kusumawati, N., P. Setiarso, S. Muslim, Q. A. Hafidha, S. A. Cahyani, and F. F. Fachrirakarsie (2024). Optimization Thickness of Photoanode Layer and Membrane as Electrolyte Trapping Medium for Improvement Dye-Sensitized Solar Cell Performance. *Science and Technology Indonesia*, **9**(1); 7–16

Liu, B., Z. Yan, T. Xu, C. Li, R. Gao, H. Hao, and J. Bai (2022). Co-Construction of Oxygen Vacancies and Heterojunctions on CeO_2 via One-Step Fe Doping for Enhanced Photocatalytic Activity in Suzuki Reaction. *Chemical Engineering Journal*, **442**; 136226

Liu, Y., H. Chen, J. Li, and P. Yang (2015). Morphology Adjustment of One Dimensional CeO_2 Nanostructures via Calcination and Their Composite with Au Nanoparticles Towards Enhanced Catalysis. *RSC Advances*, *5*(47); 37585–37591

Matussin, S. N., M. H. Harunsani, and M. M. Khan (2023). CeO_2 and CeO_2-Based Nanomaterials for Photocatalytic, Antioxidant and Antimicrobial Activities. *Journal of Rare Earths*, **41**(2); 167–181

Mohadi, R., Z. Hanafiah, H. Hermansyah, and H. Zulkifli (2017). Adsorption of Procion Red and Congo Red Dyes Using Microalgae Spirulina sp. *Science and Technology Indonesia*, **2**(4); 102–104

Mondal, K. and A. Sharma (2016). Recent Advances in Electrospun Metal-Oxide Nanofiber Based Interfaces for Electrochemical Biosensing. *RSC Advances*, **6**(97); 94595–94616

Montini, T., M. Melchionna, M. Monai, and P. Fornasiero (2016). Fundamentals and Catalytic Applications of CeO_2 -Based Materials. *Chemical Reviews*, **116**(10); 5987–6041

Mylarappa, M., S. Chandruvasan, K. S. Harisha, and K. N. Shravana Kumara (2024). Ajwain Honey Loaded CeO_2 Nanocomposite for Antioxidant, Chemical Sensors and Photocatalysis Studies. *Kuwait Journal of Science*, **51**(1); 100145

Oladoye, P. O., M. O. Bamigboye, O. D. Ogunbiyi, and M. T. Akano (2022). Toxicity and Decontamination Strategies of Congo Red Dye. *Groundwater for Sustainable Development*, **19**; 100844

Pandey, V. K., G. Ajmal, S. N. Upadhyay, and P. K. Mishra (2020). Nano-Fibrous Scaffold with Curcumin for Anti-Scar Wound Healing. *International Journal of Pharmaceutics*, **589**; 119858

Rianjanu, A., K. D. P. Marpaung, E. K. A. Melati, R. Aflaha, Y. G. Wibowo, I. P. Mahendra, and T. Taher (2024a). Integrated Adsorption and Photocatalytic Removal of Methylene Blue Dye from Aqueous Solution by Hierarchical Nb_2O_5@PAN/PVDF/ANO Composite Nanofibers. *Nano Materials Science*, **6**(1); 96–105

Rianjanu, A., K. D. P. Marpaung, C. Siburian, S. A. Muhtar, N. I. Khamidy, J. Widakdo, and T. Taher (2024b). Enhancement of Photocatalytic Activity of CeO_2 Nanorods Through Lanthanum Doping (La-CeO_2) for the Degradation of Congo Red Dyes. *Results in Engineering*, **23**; 102748

Rianjanu, A., A. S. P. Mustamin, E. K. A. Melati, R. Aflaha, N. I. Khamidy, M. Utami, and T. Taher (2024c). Photocatalytic Degradation of Aqueous Congo Red Dye Pollutants by Rare-Earth Metal Oxide (CeO_2) Nanorods. *Colloids and Surfaces A: Physicochemical and Engineering Aspects*, **682**; 132919

Rianjanu, A., R. Nuraeni, R. Aflaha, N. I. Khamidy, K. Triyana, and T. Taher (2024d). Effect of Calcination Temperature on the Performance of Hydrothermally Grown Cerium Dioxide (CeO_2) Nanorods for the Removal of Congo Red Dyes. *Greensusmater*, **1**(1); 9–14

Sriram, G., A. Bendre, E. Mariappan, T. Altalhi, M. Kigga, Y. C. Ching, and M. Kurkuri (2022). Recent Trends in the Application of Metal-Organic Frameworks (MOFs) for the Removal of Toxic Dyes and Their Removal Mechanism-a Review. *Sustainable Materials and Technologies*, **31**; e00378

Srivastava, A., R. M. Rani, D. S. Patle, and S. Kumar (2022). Emerging Bioremediation Technologies for the Treatment of Textile Wastewater Containing Synthetic Dyes: A Comprehensive Review. *Journal of Chemical Technology & Biotechnology*, **97**(1); 26–41

Sukowati, R., Y. M. Rohman, B. H. Agung, D. A. Hapidin, H. Damayanti, and K. Khairurrijal (2023). An Investigation of the Influence of Nanofibers Morphology on the Performance of QCM-Based Ethanol Vapor Sensor Utilizing Polyvinylpyrrolidone Nanofibers Active Layer. *Sensors and Actuators B: Chemical*, **386**; 133708

Tang, X., R. Tang, S. Xiong, J. Zheng, L. Li, Z. Zhou, and C. Liao (2022). Application of Natural Minerals in Photocatalytic Degradation of Organic Pollutants: A Review. *Science of The Total Environment*, **812**; 152434

Thakare, Y., S. Kore, I. Sharma, and M. Shah (2022). A Comprehensive Review on Sustainable Greener Nanoparticles for Efficient Dye Degradation. *Environmental Science and Pollution Research*, **29**(37); 55415–55436

Tkaczyk, A., K. Mitrowska, and A. Posyniak (2020). Synthetic Organic Dyes as Contaminants of the Aquatic Environment and Their Implications for Ecosystems: A Review. *Science of The Total Environment*, **717**; 137222

Yaipimai, W., N. Subjalearndee, G. Tumcharern, and V. Intasanta (2015). Multifunctional Metal and Metal Oxide

Hybrid Nanomaterials for Solar Light Photocatalyst and Antibacterial Applications. *Journal of Materials Science*, **50**(23); 7681–7697

Yan, B. and H. Zhu (2008). Controlled Synthesis of CeO_2 Nanoparticles Using Novel Amphiphilic Cerium Complex Precursors. *Journal of Nanoparticle Research*, **10**(4); 719–726

Yanalak, G., A. Aljabour, E. Aslan, F. Ozel, and I. H. Patir (2018). A Systematic Comparative Study of the Efficient Co-Catalyst-Free Photocatalytic Hydrogen Evolution by Transition Metal Oxide Nanofibers. *International Journal of Hydrogen Energy*, **43**(36); 17185–17194

Yang, F., X. Yu, Z. Liu, K. Wang, Q. Ji, Y. Chen, and B. Yao (2022). Photocatalytic Degradation Activity and Pathways of Moxifloxacin Over Metal Ion-Doped Bi_2O_3 Nanofibres Prepared Via Electrospinning. *Applied Surface Science*, **575**; 151757

Yang, X., Y. Liu, J. Li, and Y. Zhang (2019). Effects of Calcination Temperature on Morphology and Structure of CeO_2 Nanofibers and Their Photocatalytic Activity. *Materials Letters*, **241**; 76–79

Zhang, Q., X. Chen, H. Wang, X. Bai, X. Deng, Q. Yao, and S. Li (2020). Controllable Synthesis of Peapod-Like TiO_2@GO@C Electrospun Nanofiber Membranes with Enhanced Mechanical Properties and Photocatalytic Degradation Abilities Towards Methylene Blue. *New Journal of Chemistry*, **44**(9); 3755–3763

Zhao, W., M. Adeel, P. Zhang, P. Zhou, L. Huang, Y. Zhao, and Y. Rui (2022). A Critical Review on Surface-Modified Nano-Catalyst Application for the Photocatalytic Degradation of Volatile Organic Compounds. *Environmental Science: Nano*, **9**(1); 61–80

